Geophys. J. Int. (2006) **167,** 43–52 doi: 10.1111/j.1365-246X.2006.03088.x

Centennial to millennial geomagnetic secular variation

M. Korte[1] and C. G. Constable[2]

[1] *GeoForschungsZentrum Potsdam, Telegrafenberg,* 14473 *Potsdam, Germany. E-mail: monika@gfz-potsdam.de*
[2] *Institute of Geophysics and Planetary Physics, Scripps Institution of Oceanography, University of California, San Diego, La Jolla,* CA 92093-0225, *USA*

Accepted 2006 June 7. Received 2006 April 17; in original form 2005 August 12

SUMMARY

A time-varying spherical harmonic model of the palaeomagnetic field for 0–7 ka is used to investigate large-scale global geomagnetic secular variation on centennial to millennial scales. We study dipole moment evolution over the past 7 kyr, and estimate its rate of change using the Gauss coefficients of degree 1 (dipole coefficients) from the CALS7K.2 field model and by two alternative methods that confirm the robustness of the predicted variations. All methods show substantial dipole moment variation on timescales ranging from centennial to millennial. The dipole moment from CALS7K.2 has the best resolution and is able to resolve the general decrease in dipole moment seen in historical observations since about 1830. The currently observed rate of dipole decay is underestimated by CALS7K.2, but is still not extraordinarily strong in comparison to the rates of change shown by the model over the whole 7 kyr interval. Truly continuous phases of dipole decrease or increase are decadal to centennial in length rather than longer-term features. The general large-scale secular variation shows substantial changes in power in higher spherical harmonic degrees on similar timescales to the dipole. Comparisons are made between statistical variations calculated directly from CALS7K.2 and longer-term palaeosecular variation models: CALS7K.2 has lower overall variance in the dipole and quadrupole terms, but exhibits an imbalance between dispersion in g_2^1 and h_2^1, suggestive of long-term non-zonal structure in the secular variations.

Key words: archaeomagnetism, geomagnetic dipole moment, geomagnetic field models, palaeointensity, palaeosecular variation.

1 INTRODUCTION

Global time-varying field models based on current and historical geomagnetic observations have been widely used to study the geomagnetic secular variation on decadal to centennial timescales (e.g. Bloxham *et al.* 1989; Bloxham & Jackson 1992; Jackson *et al.* 2000; Hulot *et al.* 2002; Finlay & Jackson 2003). Such secular variation studies have naturally focused on the physical processes that are considered dominant on these relatively short timescales, leading to an emphasis on linking secular variation to decadal changes in length of day, geomagnetic jerks, torsional oscillations, searches for evidence for Ohmic diffusion, and the nature of fluid flow at the core–mantle boundary. The picture that emerges for the past 400 yr is of stable large-scale spatial structure in the geomagnetic field, and of secular variation that appears more intense and smaller in both spatial and temporal scales in longitudes extending from about 100°W to 120°E than that in the Pacific region. The anomalous behaviour in the Pacific has been correlated with seismic evidence for thermal anomalies in the lowermost mantle (e.g. Masters *et al.* 1996), and has been interpreted as a sign that geographically heterogeneous thermal and possibly chemical boundary conditions may have a detectable influence on the long-term (millennial to million year) spatial structure and/or secular variation and reversals of the geomagnetic field (Cox & Doell 1964; Bloxham & Gubbins 1987; Laj *et al.* 1991; Gubbins 1998; Johnson & Constable 1998; Costin & Buffett 2004; Gubbins & Gibbons 2004). The detection of anomalous time-averaged fields and secular variation from the palaeomagnetic record during the period 0–5 Ma remains a topic for current debate (e.g. McElhinny 2004).

Since systematic global measurements were begun about 175 yr ago, there has also been a steady decrease in the dipole strength at a rate of about 5 per cent per century. The decrease may be linked mechanistically to geomagnetic reversals (Gubbins 1987), and has led to some concerns that we might be observing at the early stages of a reversal (Hulot *et al.* 2002; Olson 2002). Although the rate is rapid (about 5 times as fast) compared with that expected for free decay of the field if the geodynamo ceased operation, the historical record is too short to allow inferences about continued decay of the field or the likelihood of geomagnetic reversal based on these data alone. Two other sources of information that can be exploited for this purpose are the output from numerical dynamo simulations and palaeomagnetic observations. Both these are, in principle, also useful for studies of longer-term geomagnetic secular variation on a broad range of spatial and temporal scales.

The current dipole decay rate and accompanying increase in complexity of the geomagnetic field do agree with features shown by

some numerical dynamo models in the early stages of reversal. However, even though some of these numerical dynamos show Earth-like field behaviour, their parameter ranges remain far from those considered appropriate for the Earth (Dormy *et al.* 2000) and the agreement may be coincidental. The physical origins of geodynamo variations on many timescales are still not well understood (Hollerbach 2003), and it remains a significant challenge to relate the output of numerical simulation to palaeomagnetic observations (see Kono & Roberts 2002, for a review). Any comparisons must rely on the evaluation of statistical properties of the palaeofield and the simulations. The most fruitful of those currently being explored consider the symmetry properties of the geodynamo [originating from work by Young (1974) and Gubbins (1975) and reviewed in the palaeomagnetic context by Gubbins (1998)], including symmetry or antisymmetry of the palaeofield about the equator (McFadden *et al.* 1988; Tauxe & Kent 2004), axial symmetry (Constable & Johnson 1999), and the more general symmetry properties considered in some detail by Hulot & Bouligand (2005) (see also Bouligand *et al.* 2005). In these comparisons, the global palaeofield variations are generally described in terms of the statistical distributions of the spherical harmonic coefficients that represent the spatial structure of the field, the distributional variability arising from the temporal variations of the palaeomagnetic field (Constable & Parker 1988b).

In this work, we use a recently developed time-varying palaeomagnetic field model, CALS7K.2 (Korte & Constable 2005b), to study both dipole moment variability and long-wavelength secular variation on centennial to millennial timescales, with a view to bridging the gap between the historical record and statistical studies on million year timescales.

In Section 2, we discuss the results of a high-resolution study of the past variability of the geomagnetic dipole moment. The temporal development in terms of splines allows a direct estimate of the rate of change of dipole moment, with higher resolution than earlier palaeomagnetic results derived solely from virtual axial dipole moments (VADMs) (McElhinny & Senanayake 1982; Yang *et al.* 2000). Detailed studies of the dipole moment allow the evaluation of the current dipole moment decrease in a longer-term context, and are also essential for studies of solar variability and palaeoclimate based on past cosmogenic nuclide production (e.g. Elsasser *et al.* 1956; Stuiver *et al.* 1991; Solanki *et al.* 2004).

Section 3 is concerned with analysis of the large-scale secular variation manifested by CALS7K.2, including terms up to degree 5. We consider the distribution of power in the secular variation in both time and space and the evidence for non-zonal structure in the geomagnetic field and its secular variation. The statistical and symmetry properties of the Gauss coefficients from CALS7K.2 are compared with those from two recent palaeosecular variation (PSV) models.

2 DIPOLE MOMENT VARIABILITY

Details of the CALS7K.2 model have been presented elsewhere (Korte & Constable 2005b), so here we simply note that the modelling techniques are similar to those commonly used for the modern field (Bloxham & Jackson 1992; Jackson *et al.* 2000). CALS7K.2 is a spatially and temporally regularized spherical harmonic model extending to degree and order 10, and its temporal development is parametrized by B-splines with a knot spacing of 55 yr. The model covers the time interval 5000 BC to 1950 AD, and is based on directional data derived from lake sediments and both directional and absolute palaeointensity data from archaeological artefacts and young lava flows (Korte *et al.* 2005). Spatial and temporal regularization is necessary to avoid overfitting of data with high uncertainties and spurious structure in areas sparsely covered by data, particularly the Southern Hemisphere. As a consequence, the temporal and spatial resolutions of CALS7K.2 are no better than 100 yr and degree and order 5, respectively, with short-term and small-scale field features being smoothed significantly by the regularization. The notation used here is such that at any time t, CALS7K.2 is described by a suite of time-varying Gauss coefficients $g_l^m(t)$ and $h_l^m(t)$ with degree l, $1 \le l \le 10$, and order m, $0 \le m \le l$.

At present, a centred dipole with a moment of 7.78×10^{22} Am^2 and tilted by about 11° relative to the Earth's axis accounts for 93.7 per cent of the power observed at the Earth's surface. In the geomagnetic context, we take power to mean the average of the squared magnetic field strength, B^2, over the Earth's surface. This can be specified as a function of spherical harmonic degree and is then commonly referred to as the spatial geomagnetic power spectrum (Lowes 1974). CALS7K.2 allows us to make direct comparisons with the results obtained by current models, and we find that averaged over the past 7 kyr the dipole remains dominant contributing almost 98 per cent of average power. In the past, ancient dipole strength has commonly been studied using VADMs, obtained from palaeomagnetic intensity results (Valet 2003). VADMs do not take account of non-dipole field contributions and to minimize that influence they are usually averaged over at least a few centuries. The temporal resolution of VADM studies of this kind for the past 12 millennia (McElhinny & Senanayake 1982; Yang *et al.* 2000) is therefore limited, and as we recently showed (Korte & Constable 2005a), the resulting VADM estimates are also systematically higher than the dipole moment from CALS7K.2. In that work, we were able to show that there is no inconsistency between the two sets of results: the differences are attributable to data quality and to non-dipole field contributions that are aggravated by the available geographical sampling and persist in the averaged VADMs. In this section, we investigate rates of change of the dipole moment using both the dipole moment from CALS7K.2 and the VADMs that have traditionally been used in such analyses. Note that, strictly speaking, we should compare VADMs to the purely axial dipole moment or use virtual dipole moments (VDMs), taking into account the dipole tilt, for comparison to the full dipole moment. However, the differences both between dipole moment and axial dipole moment and between VDMs and VADMs are small in general and insignificantly small with respect to the resolution of the CALS7K.2 model.

2.1 Virtual axial dipole moments

We begin by seeking a high-resolution estimate of temporal changes in the VADM, because the commonly used averaging of individual VADMs over several centuries significantly limits the temporal resolution of the result. First, we fit a smoothing spline (Constable & Parker 1988a) to the VADMs determined from the subset of 3092 data points from the archeointensity compilation used in CALS7K.2, according to the following transformation:

$$\mathrm{VADM} = \frac{4\pi a^3}{\mu_0} B(1 + 3\cos^2\theta)^{-1/2} \quad (1)$$

with $a = 6371.2$ km the average radius of the Earth, $\mu_0 = 4\pi \times 10^{-7}$ $Vs/(\mathrm{A\ m})$ the permeability of free space, and θ the colatitude of the location for which the field strength B was obtained. The maximum temporal variability that the smoothing spline can represent is governed by the number of knot points and the quality of the fit to the data. The spline should represent all variations required by

the data, and the variability should not be limited by the knot point interval. The chosen interval of ∼23 yr ensures this. The averaging of the non-dipole field in this case comes from the quasi-global coverage, and the temporal resolution achieved by the regularization of the spline.

Two spline fits to the VADM data are presented here. A weighted spline was obtained with the data weighted by their uncertainty estimates, which were determined from the total uncertainty estimates (data and dating) of the intensity data used in producing the CALS7K.2 model. The spline was fitted with a normalized rms misfit of 1.0, that is, the data were fitted to the expected value of χ^2 based on their uncertainties. In order to evaluate the influence of our uncertainty estimates, we also fitted an unweighted spline for which the rms misfit was chosen to roughly reflect the standard deviation of the 1000-yr averages and is 1.66×10^{22} A m^2. Both these splines are shown together with the individual VADMs and their 1000- and 500-yr averages for the intervals 5000 BC–2000 BC and 1000 BC–1950 AD, respectively, in Fig. 1(a). Weighting the VADMs by their uncertainty estimates decreases the magnitude of the resulting curve in the time-span of highest dipole moment, where the scatter and error estimates are highest. The main temporal structure, however, is robust and (apart from the expected bias in magnitude caused by the influence of non-dipole contributions and uncertainties in the data) agrees reasonably well with the dipole moment M predicted from CALS7K.2, namely

$$M(t) = \left\{ \frac{4\pi a^3}{\mu_0} \sqrt{\left[g_1^0(t)\right]^2 + \left[g_1^1(t)\right]^2 + \left[h_1^1(t)\right]^2} \right\}. \quad (2)$$

Both splines and the dipole moment are displayed in Fig. 1(b) together with VADM results predicted from the CALS7K.2 model at times and locations of the data points. VADM estimates (black dots, red and blue line) are almost all significantly higher than the dipole moment prediction from the spherical harmonic model CALS7K.2 (black line), although the VADM results (grey) predicted from the model at times and locations of data points mainly agree with VADM spline estimates. The main differences occur when the dipole moment is low, but non-dipole contributions are high (Korte & Constable 2005b).

2.2 Spherical harmonic descriptions

One of the significant improvements in the CALS-family models compared to previous modelling efforts for these time-spans is the use of a physical regularization instead of a simple truncation of the

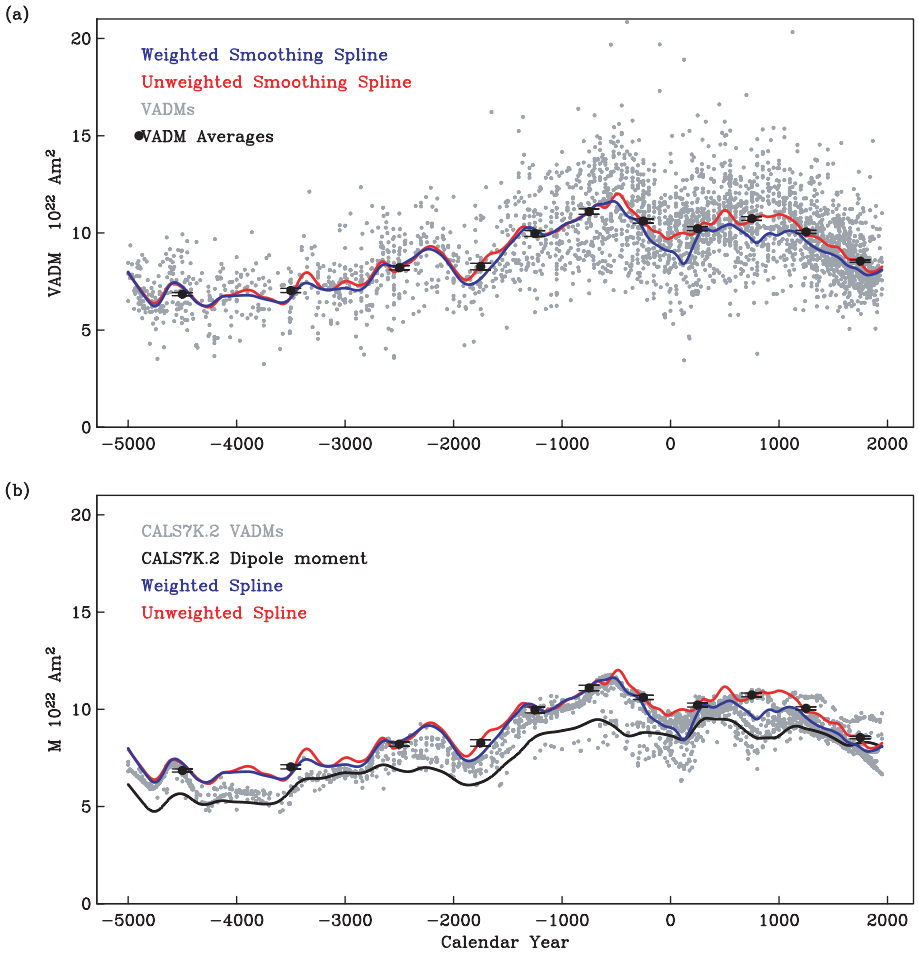

Figure 1. Virtual axial dipole moments (VADMs). (a) Individual VADM results (grey) used in CALS7K.2 and various dipole moment estimates based on them: 1000- and 500-yr averages (black, 5000 BC–2000 BC and 1000 BC–1950 AD, respectively) with one standard error uncertainties in the mean, spline fit (red) to the VADMs, spline fit to the VADMs (blue) weighted by the uncertainty estimates described in Korte *et al.* (2005). (b) VADM estimates (black dots, red and blue line) are almost all significantly higher than the dipole moment prediction from the spherical harmonic model CALS7K.2 (black line), although the VADM results (grey) predicted from the model at times and locations of data points mainly agree with VADM spline estimates. The main differences occur when the dipole moment is low, but non-dipole contributions are high (Korte & Constable 2005b).

spherical harmonic series at low degrees and orders. However, it is possible to model the data allowing only a dipole in the spatial representation, that is, a truncation of the spherical harmonic expansion right after degree and order 1. Although this violates the philosophy of finding out how much spatial field structure is required by the data, a dipole-only inversion can be a useful exercise in studying dipole variability and the influence of the non-dipole contributions. It avoids the use of spatial regularization and prevents this from influencing the allowed temporal variability in the dipole. We therefore decided to try this exercise. We use the depleted data set underlying CALS7K.2 (after the iterative data rejection, see Korte & Constable 2005b) for a dipole-only inversion. The modelling method is the same as used for CALS7K.2, except that the spatial expansion is truncated at degree and order 1 and consequently no spatial damping is necessary. The knot-point spacing of the temporal splines and the weighting of the intensity data are the same as for CALS7K.2. An rms misfit of 1.0 could not be achieved with such a simple model (indicating the need for non-dipole terms in the field description) and the normalized rms misfit of the estimate shown in Fig. 2(a) is 1.3, resulting from four iterations with a temporal damping factor of 0.1 nT^{-2} yr^4.

To determine the reliability of each of the spherical harmonic dipole moment estimates and temporal variation, we applied a bootstrap resampling method to the modelling. Based on the original depleted data set underlying CALS7K.2, 3000, data sets with an identical number of data randomly drawn from the original set were created. The bootstrap considers each datum separately in the resampling approach (so that it is likely that for lake sediments at most a handful of data might be omitted from each location, but not a whole time-series), and this allows the ratio of directional and intensity data to vary slightly among the bootstrap sample data sets.

All data sets were modelled with the same parameters and numbers of iterations as for the original CALS7K.2 and dipole-only models, respectively. The standard deviations obtained this way for the dipole moment are quite small, as shown in Fig. 2(a). They represent uncertainty estimates based on the information content contained in the currently available data and probably are somewhat optimistic.

There is good agreement among the commonly used average VADMs, our spline fit and the dipole moment obtained from this intensity and directional data fit to a time-varying, tilted dipole. The truncation of this spherical harmonic expansion at degree and order 1 biases the result by spatial aliasing, which is a comparable effect to the influence of the non-dipole contributions in VADMs. The centennial-scale variability of our various dipole moment

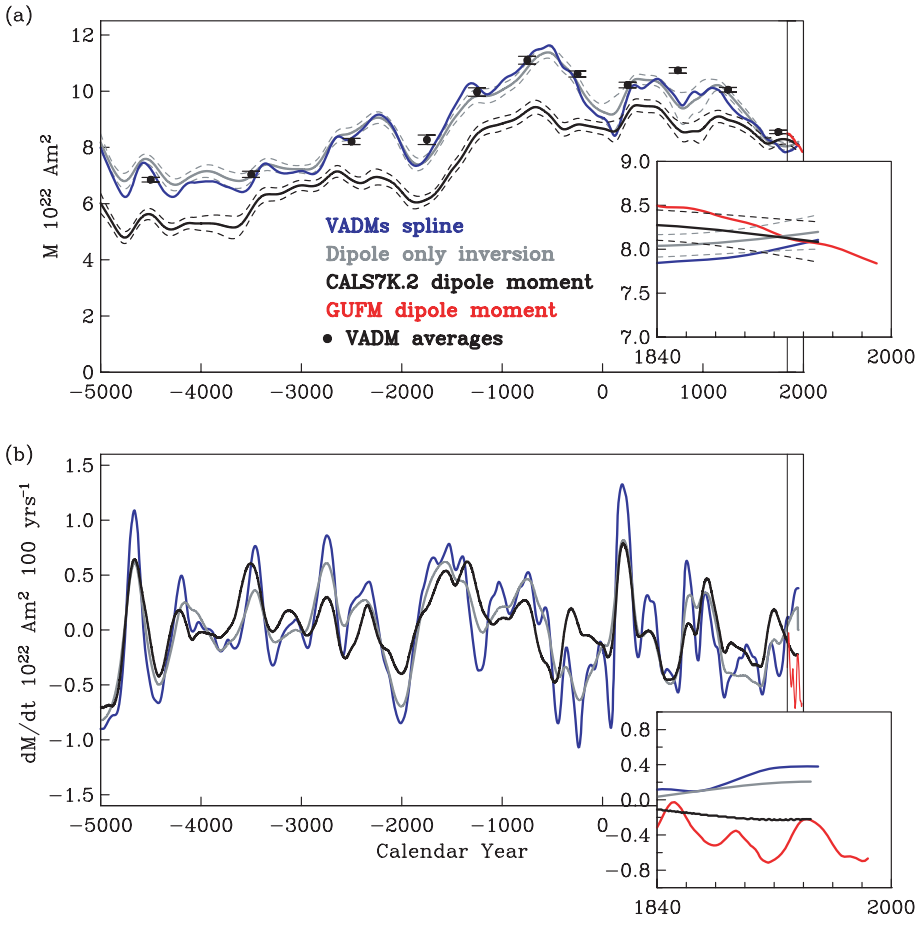

Figure 2. Dipole moment variability. (a) Dipole moment estimates (M) and (b) their rates of change for the past 7000 yr obtained from the same data by different methods: average VADMs (black dots) and weighted spline fit (blue line) from Fig. 1, spherical harmonic inversion of intensity and directional data for a dipole-only (grey line), dipole moment estimate from CALS7K.2 (black line) and in the expanded right-hand part also from the historical model GUFM (red, Jackson *et al.* 2000). Uncertainty estimates for the spherical harmonic models were determined by a bootstrap method, with the dashed lines giving one standard error. The agreement in most of the temporal structure is confirmed by the general accordance between rates of change per century for VADM spline and spherical harmonic dipole moments in (b).

predictions is quite robust, although the temporal resolution is not as good as in modern geomagnetic field models.

The use of cubic splines for the temporal parametrization allows a direct calculation of the rates of change in the various dipole estimates, and these are plotted together in Fig. 2(b). We expect that among these estimates CALS7K.2 gives the most-reliable estimate for dM/dt: nevertheless, there is a surprising level of agreement among all the estimates. The lower resolution achievable in palaeomagnetic versus historical models is clearly seen from the rates of change in Fig. 2(b) in comparison to those from the 1590–1990 AD GUFM model (Jackson *et al.* 2000) in the overlapping time interval. Among the continuous palaeomagnetic estimates, only CALS7K.2 is able to resolve at all the current decrease of the dipole seen since 1840 in the historical model GUFM (Jackson *et al.* 2000) as well as in other models from current data. The disagreement between the CALS7K.2 and GUFM dipole moments around 1850 is almost certainly due to this limited resolution and the fact that CALS7K.2 simply does not fully resolve a temporary dipole maximum. The CALS7K.2 dipole prediction in Fig. 2(a) shows that between about 1650 and 1800 there is an interruption in the steady decrease of dipole moment, with the rate of change still being close to 0 around 1840. This result has been confirmed in a recent study by Gubbins *et al.* (2006), who estimated a constant rate of change in the axial dipole coefficient that is indistinguishable from zero for the time-span 1590–1990. This result is derived directly from palaeointensity data and differs considerably from the extrapolation used in GUFM for that time interval. Although the estimation techniques differ significantly, the palaeointensity data and associated error estimates used in that study are exactly the same as in the equivalent time interval of CALS7K.2.

3 LARGE-SCALE SECULAR VARIATION FOR 0–7 KA

3.1 Spatial power variability

We turn now to an investigation of the large-scale secular variation of the field, including the non-dipole contributions to CALS7K.2. We noted earlier that secular variation causes temporal changes in the spatial power distribution (Korte & Constable 2005b), so we begin by looking at how R_l, the spatial power at each spherical harmonic degree, varies with time t. R_l is the average squared field B at spherical harmonic degree l at the Earth's surface (Lowes 1974), that is,

$$R_l(t) = \langle \mathbf{B}_l(t) \cdot \mathbf{B}_l(t) \rangle_{r=a} = (l+1) \sum_{m=0}^{l} \left\{ \left[g_l^m(t) \right]^2 + \left[h_l^m(t) \right]^2 \right\}. \tag{3}$$

We limit this analysis to no more than degree 5, beyond which the model clearly lacks resolution and the regularization dominates.

Fig. 3(a) shows the temporal development of power in each spherical harmonic degree at the Earth's surface, together with the mean spectrum and the dispersion about the mean. The dispersion which reflects the amplitude of the variations is just the standard deviation of each R_l about its mean, but should not be confused with an uncertainty estimate. It is more or less proportional to l, but relative to the mean value is smallest in the dipole and strongest in the octupole (Table 1). The increasing similarity in temporal evolution of R_l at higher degrees (a feature which continues in degrees 6 to 10 which are not shown here) must be attributed to the regularization in the model. The variability in degree 4 and 5 may already be damped to a

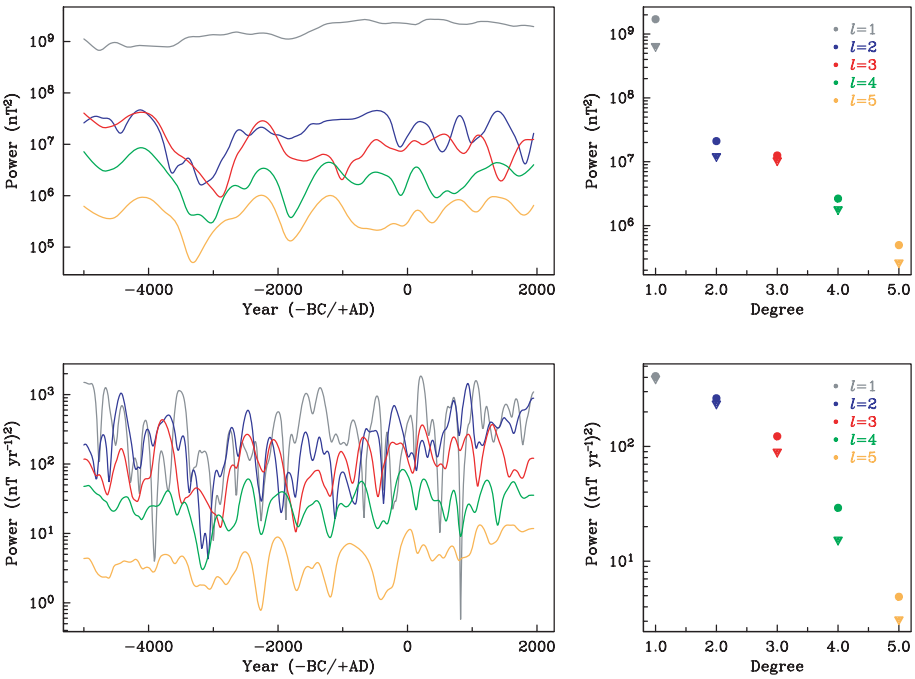

Figure 3. (a) Temporal development of degree l power in CALS7K.2 together with the power spectrum at the Earth's surface including the dispersion (triangles) about the mean (dots). (b) The same for secular variation power.

Table 1. Mean spectral powers R_l and S_l with dispersions as a measure for variability of the field and secular variation, respectively.

Degree l	R_l (nT^2)	Dispersion R_l (per cent)	S_l [(nT yr^{-1})^2]	Dispersion S_l (per cent)
1	$1.708\,28 \times 10^9$	38	410	95
2	2.105×10^7	58	263	90
3	1.254×10^7	84	123	73
4	2.65×10^6	68	29	53
5	4.9×10^5	53	5	63

certain degree by the spatial regularization, which means that while the relative dispersion in the quadrupole clearly is lower than that in the octupole we cannot say this with certainty about the higher degrees. Keep in mind also that we are looking only at the past 7 kyr here. Over (much) longer periods the dispersion in the dipole must be higher to allow for field reversals.

In Fig. 3(b), the secular variation power in each degree with time is displayed and the temporal variability is characterized by the secular variation spectrum, again including the variance about the mean power in each degree. Note that while Figs 2(b) and 3(b) both contain information about the amount of change in the field per time interval, they were obtained in different ways. The rate of change of the dipole moment M shown in the previous section is given by

$$\frac{dM}{dt} = \frac{d}{dt}\left[\frac{4\pi a^3}{\mu_0}\sqrt{\left(g_1^0\right)^2 + \left(g_1^1\right)^2 + \left(h_1^1\right)^2}\right], \tag{4}$$

while the secular variation power S_l in each degree l is

$$S_l = \left\langle \frac{\mathbf{B}_l(t)}{dt} \cdot \frac{\mathbf{B}_l(t)}{dt} \right\rangle_{r=a} = (l+1)\sum_{m=0}^{l}\left\{\left[\frac{d\left(g_l^m\right)}{dt}\right]^2 + \left[\frac{d\left(h_l^m\right)}{dt}\right]^2\right\}. \tag{5}$$

The secular variation power thus includes no information about the sign of the field change. It is obvious that the dipole secular variation $S_1(t)$ is at least as dynamic as that of the higher degrees on all timescales of variation, and Table 1 shows that relative to the mean it is highest.

3.2 Statistical models

Looking at the power and variability per spherical harmonic degree as we have done so far seems reasonable because the degree determines the spatial wavelength. Partitioning the power as a function of l according to what is seen in the modern field is also a strategy that has been widely used in modelling the PSV on very long timescales. PSV studies are usually based on global collections of palaeomagnetic directions derived from lava flows whose precise temporal ordering is often unknown. It is not possible to derive a time-dependent spherical harmonic model like CALS7K.2 from these data. Instead the model is described by a collection of Gaussian distributions, one for each individual spherical harmonic coefficient: the mean of each distribution gives the long-term average for the spherical harmonic coefficient, and the variance about the mean represents the overall magnitude of the time variations without regards for any specific ordering. Such models, termed Giant Gaussian Processes (GGPs) (Constable & Parker 1988b), have generally disregarded any temporal correlations and frequency content in the signal, although, in principle, it is possible to include temporal correlations in such a process (Hulot & LeMouël 1994). Various simplifying assumptions can be made in constructing GGPs involving the symmetry of the geomagnetic field, and then tested for compatibility with the observations. Spherical symmetry is easily rejected in both the average and PSV because of the dominance of the axial dipole. Two other symmetries that have received consideration are equatorial and axisymmetry. See Hulot & Bouligand (2005) for an up-to-date discussion.

Equatorially symmetric (ES) contributions to the field potential are described by spherical harmonics with $l - m$ even, and equatorially antisymmetric (EA) by $l - m$ odd. One recent PSV model, TK03 (Tauxe & Kent 2004), supposes that the ES and EA terms have different amounts of variability, but each follows a specific functional form corresponding to a spatial power spectrum that is white over all degrees at the core–mantle boundary. The dispersions for TK03 up to degree and order 3 are shown in Fig. 4, where it is seen that the antisymmetric terms ($l - m$ odd) have a dispersion 3.8 times as large as the symmetric ones for the same degree l. In axisymmetric models (like TK03), all pairs of non-zonal Gauss coefficients with the same degree l and order m have the same dispersion. The CJ98 model (Constable & Johnson 1999) also shown in Fig. 4 is axisymmetric too, but in common with earlier models (e.g. Kono & Tanaka 1995; Hulot & Gallet 1996; Quidelleur & Courtillot 1996) follows a different approach from TK03. Deviations from a white spectrum are introduced for specific Gauss coefficients in order to fit the observations: In CJ98, this results in high dispersion in g_1^0, g_2^1 and h_2^1, and relatively low values in g_1^1 and h_1^1. Although the dispersions for these two models appear quite different, they fit the palaeomagnetic directional data from lavas about equally well in part because the magnitude of the standard deviation or dispersions is effectively scaled by the average size of g_1^0 (see Table 2).

With CALS7K.2, we can estimate the statistics for the Gauss coefficients directly, so in Fig. 4 we compare the dispersion of the individual dipole, quadrupole and octupole coefficients of CALS7K.2 with those for the two statistical palaeomagnetic models TK03 and CJ98. The dispersion, in fact again the standard deviation of the coefficients' time-series, is a measure of the amplitude of variations

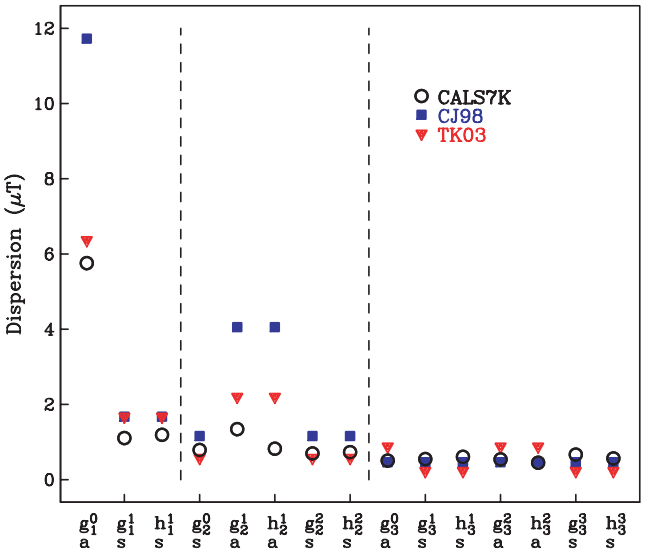

Figure 4. Dispersion in spherical harmonic coefficients of CALS7K.2 (Korte & Constable 2005b) and the statistical models CJ98 (Constable & Johnson 1999) and TK03 (Tauxe & Kent 2004) for dipole, quadrupole and octupole. The annotations 'a' and 's' denote equatorially antisymmetric and symmetric coefficients.

Table 2. Average coefficients and their dispersion in μT for CALS7K.2 and two statistical models.

Coefficient			CALS7K.1		CJ98		TK03	
	l	m	Average	Dispersion	Average	Dispersion	Average	Dispersion
g	1	0	−28.6	5.76	−30	11.72	−18	6.37
g	1	1	−0.33	1.11	0	1.68	0	1.68
h	1	1	0.51	1.19	0	1.68	0	1.68
g	2	0	−1.66	0.79	−1.5	1.16	0	0.58
g	2	1	−0.24	1.34	0	4.06	0	2.20
h	2	1	−0.01	0.82	0	4.06	0	2.20
g	2	2	0.42	0.70	0	1.16	0	0.58
h	2	2	0.23	0.73	0	1.16	0	0.58
g	3	0	−0.14	0.51	0	0.46	0	0.88
g	3	1	−0.24	0.55	0	0.46	0	0.23
h	3	1	−0.50	0.61	0	0.46	0	0.23
g	3	2	0.33	0.54	0	0.46	0	0.88
h	3	2	−0.19	0.45	0	0.46	0	0.88
g	3	3	−0.39	0.67	0	0.46	0	0.23
h	3	3	−0.55	0.57	0	0.46	0	0.23

in each coefficient. The dispersion in dipole and quadrupole terms is generally lower in CALS7K.2 than in the palaeomagnetic models, which might reflect the shorter time interval of only 7 kyr in CALS7K.2 versus millions of years in the statistical models. The dispersion in CALS7K.2 might also be damped by the regularization due to the lower temporal resolution, poor data distribution and lower data quality, but we would expect this to have a stronger influence on the higher degrees and consider it to be of only minor influence in dipole and quadrupole. CALS7K.2 in dipole and quadrupole clearly shows similar dispersions to the statistical models with the highest dispersion in the axial dipole and high dispersion in the $m = 1$ coefficients for both degrees. It is not clear, however, whether the behaviour of CALS7K.2 is closer to CJ98 or TK03. In the octupole, the dispersion in the CALS7K.2 coefficients is not higher in the EA than that in the ES parts, but neither is it uniform across all values of m. A striking difference is seen between the dispersions of the quadrupole order 1 coefficients, which are equal for g_2^1 and h_2^1 in the statistical models but not in CALS7K.2, which might reflect axial asymmetry in the field evolution. Such axial asymmetry was included in CJ98.nz, a non-zonal version of CJ98, but was not required to fit the palaeomagnetic data used in those models. The average values of the coefficients themselves, listed in Table 2, are a measure for the deviation of the time-averaged field from an axial dipole. Most of the average coefficients except for the axial dipole are small in CALS7K.2: we note that the largest value occurs for g_2^0, which implies a zonal structure and (as noted by Hulot & Bouligand 2005) equatorial symmetry breaking when combined with the average axial dipole field. The observed value for g_2^0 is close to that used in the CJ98 model.

3.3 Spectral content of CALS7K.2

To gain better insight into the timescales of large-scale secular variation, we calculated power spectral densities as a function of frequency for each $R_l(t)$ time-series and for the individual Gauss coefficients up to the axial octupole g_3^0. We cannot make any physical interpretations at periods less than 55 yr (0.018 yr^{-1}), the knot-point spacing of the temporal spline basis functions, so the spectra displayed in Fig. 5 are cut off at 0.018 yr^{-1}. The frequency spectra for R_l (Fig. 5a) show generally similar, quite rapid fall-off for each degree. The flattening of the higher-degree spectra at high frequency is due to the beginning influence of the knot spacing. No special periodicities are detected but octupole and higher degrees have most power at periods between 1000 and 2000 yr. As we saw earlier, the temporal power is roughly proportional to the spatial power, except for quadrupole and octupole. In the quadrupole, there is less power in the periods of a few millennia and significantly more power at about 500 yr. Looking at the temporal spectra of individual Gauss coefficients (Fig. 5b), however, reveals a more complicated field behaviour: the axial dipole (g_1^0) also has most power at periods of 1000–2000 yr, which is not seen in the complete, tilted dipole because the equatorial dipole contributions have most power at long periods with a continuous fall-off towards higher frequencies. The zonal contributions and h_2^1 are responsible for the high power around a period of 1000 yr in quadrupole and octupole.

An approach which could lead to a better understanding of secular variation mechanisms is to look for frequency-dependent correlations among the coefficients used to describe the field. This could help to identify axial or zonal symmetries or systematic changes like westward drift which might allow inferences about the underlying physical processes. For this purpose, we used the variation of the minimum bias multitaper spectral methods described by Riedel & Siderenko (1995) and used in the palaeomagnetic context (see Constable *et al.* 1998; Constable & Johnson 2005) to study power spectra and coherence among various rock and palaeomagnetic properties of marine sediment cores. The results we obtain from the analysis of CALS7K.2 are as follows. First, we checked for large-scale symmetries, using spatial power time-series for EA and ES, zonal and non-zonal, and dipole and non-dipole contributions. No significant coherence exists between zonal and non-zonal field contributions but we noted a weak coherence above the significance level between ES and EA parts of R_l at periods of about 80 and 130 yr. Both the zonal and EA field contributions are strongly dominated by the axial dipole and it turns out that the observed coherence is purely between axial dipole and ES field contributions; there is no coherence between non-axial dipole EA and the ES contributions. Coming back to the zonal field contributions, the correlation analysis shows coherence well above the significance level between the axial dipole power and the non-dipole zonal power, but only for most of the period range between 400 and 100 yr and not the longer periods. Looking once more at individual coefficients instead of degree power, it turns out this is a correlation only between dipole and quadrupole zonal contributions, which are in phase over the period range from 400 down to the resolution limit of 55 yr. Coherences in the same period range are also found between axial dipole (g_1^0) and g_2^1, g_3^1, respectively. Coherences above the significance level

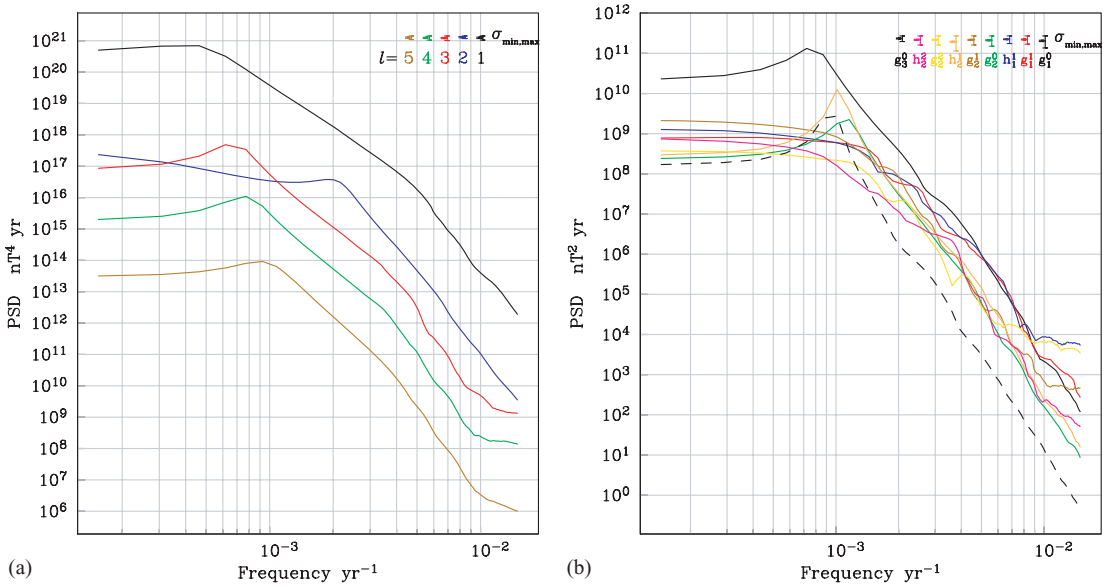

Figure 5. Power spectral densities of spherical harmonic degree l power (a) and individual coefficients (b) of CALS7K.2. The spectra are cut off at the period of 55 yr, the knot-point spacing of the temporal spline basis functions.

on the century timescale also exist between g_1^1 and g_2^1, h_1^1 and h_2^1, g_2^1 and g_3^1, h_2^1 and h_3^1, g_2^1 and g_3^2, and h_2^1 and h_3^2. Such correlations among variations in the Gauss coefficients have been contemplated in discussions of PSV models (Hulot & Gallet 1996).

4 CONCLUSIONS

4.1 Dipole secular variation

Our comparison between dipole and higher-degree variation has shown that significant short-period variations exist in the geomagnetic dipole moment and even in the axial dipole, which had not been resolved by the previously used VADMs averaged over 500–1000 yr (McElhinny & Senanayake 1982; Yang *et al.* 2000). An implicit assumption in using VADMs averaged over a few hundred years to represent actual dipole behaviour is that the variability of the non-dipole contributions is greater on short timescales than that of the dipole itself, and that temporal averaging will efficiently remove the non-dipole contributions. Our analysis has shown that this is not the case. This shorter-term variability of the dipole moment is important, and should, for example, be taken into account in studying solar irradiation and climate changes from cosmogenic nuclide production rates.

The dipole moment during the past 7000 yr shows a distinctive long-term behaviour, with low values in the earlier half and high values in the recent half of that period, giving an average close to the current value. The values in the earlier half, however, are close to the long-term palaeomagnetic average VADMs of 5.9×10^{22} A m^2 for the past 800 kyr (Valet 2003) and 4.5×10^{22} A m^2 for the past 160 Myr (Tauxe 2006). One cannot discount the possibility that the long-term average VADMs also suffer from unknown bias. The current dipole moment decrease is far from monotonic, but appears to be part of a general process lasting for about 2650 or 1650 yr now, depending on how we judge the period around 0 AD between the two maxima. The rates of change (Fig. 2b) vary significantly and truly continuous decreases or increases are decadal to centennial, rather than millennial features. The average rate of decrease since 350 AD is about 1.5 per cent per century, significantly lower than the current 5 per cent per century and only slightly higher than the free decay rate of about 1 per cent per century. The rate for the current decrease is strong, but easily within the range observed during the past seven millennia. A continuing nearly linear decay over more than a few centuries seems unlikely, as there is only one interval in which the average field increases over more than 1000 yr. Future improvements in resolution may lead to revisions of the longevity of this feature.

4.2 Secular variation features of quadrupole and octupole field contributions

The lower dispersion in dipole and quadrupole coefficients in CALS7K.2 than in statistical palaeomagnetic models might reflect the shorter time interval of CALS7K.2. This implies that lower-frequency variations exist and contradicts a conclusion by Hongre *et al.* (1998) that the typical timescales involved in spherical harmonic degree 2 (and 3) are of the order of a few centuries only and there is no correlation over more than about 450 yr. Our inference is supported by the result that axial quadrupole, octupole and h_2^1 show significant power at periods of about 1000 yr. The time interval of 2000 yr studied by Hongre *et al.* (1998) might just have been too short to reveal periodicities longer than half a millennium. However, our analysis does confirm that g_2^0 does not average to zero over several millennia as had been found by Hongre *et al.* (1998) and is compatible with what is seen in time-averaged palaeomagnetic models. This means that the averaged field is not simply equatorially antisymmetric but zonal structure and equatorial symmetry breaking have to be expected in long-time averages.

4.3 Symmetries on millennial and palaeomagnetic timescales

A clear difference between the 7000 yr model CALS7K.2 and the longer-term PSV models is seen in the dispersions of the order 1 quadrupole coefficients, which are unequal for g_2^1 and h_2^1 in CALS7K.2. While the PSV data have been explained by a zonal

average model, the millennial scale model requires some axial asymmetry, which might reflect the low secular variation observed in the Pacific region and imply a timescale of at least a few millennia for this feature. The correlation seen between g_1^0 and g_2^1, g_3^1 respectively also could be an indication for this persistent asymmetry, of which we cannot tell the timescale. Further coherences between individual coefficients of CALS7K.2 are rather inconclusive and hard to interpret in terms of symmetry. As they are rather weak, they may not prove robust over longer timescales.

ACKNOWLEDGMENTS

We wish to thank Agnès Genevey for compiling and carefully checking the global intensity data set used to determine the VADMs and the spherical harmonic models. Discussions with her contributed significantly to our efforts of assigning consistent uncertainties to all the data from different sources. The power spectral densities were conveniently determined by the programs PSD and CROSS, for which we thank Bob Parker. Constructive comments from two anonymous reviewers and Richard Holme are gratefully acknowledged. This work was partly funded by US National Science Foundation (EAR0337712 and EAR0537986) and facilitated by support from Alexander von Humboldt Foundation under the follow-up sponsorship programme.

REFERENCES

Bloxham, J. & Gubbins, D., 1987. Thermal core-mantle interactions, *Nature,* **325,** 511–513.

Bloxham, J. & Jackson, A., 1992. Time-dependent mapping of the magnetic field at the core-mantle boundary, *J. geophys. Res.,* **97,** 19 537–19 563.

Bloxham, J., Gubbins, D. & Jackson, A., 1989. Geomagnetic secular variation, *Phil. Trans. R. Soc. Lond. Ser. A,* **92,** 415–502.

Bouligand, C., Hulot, G., Khokhlov, A. & Glatzmaier, G., 2005. Statistical palaeomagnetic field modelling and dynamo numerical simulation, *Geophys. J. Int.,* **161,** 603–626.

Constable, C. & Johnson, C., 1999. Anisotropic paleosecular variation models: Implications for geomagnetic observables, *Phys. Earth planet. Inter.,* **115,** 35–51.

Constable, C. & Johnson, C., 2005. A paleomagnetic power spectrum, *Phys. Earth planet. Inter.,* **153,** 61–73, doi:10.1016/j.pepi.2005.03.015.

Constable, C.G. & Parker, R.L., 1988a. Smoothing, splines and smoothing splines: Their application in geomagnetism, *J. Comput. Phys.,* **78,** 493–508.

Constable, C.G. & Parker, R.L., 1988b. Statistics of the geomagnetic secular variation for the past 5 Ma, *J. geophys. Res.,* **93,** 11 569–11 582.

Constable, C., Tauxe, L. & Parker, R., 1998. Analysis of 11 Myr of geomagnetic intensity variation, *J. geophys. Res.,* **103,** 17 735–17 748.

Costin, S. & Buffett, B., 2004. Preferred reversal paths caused by a heterogeneous conducting layer at the base of the mantle, *J. geophys. Res.,* **109**(6), B06101, doi:10.1029/2003JB002853.

Cox, A. & Doell, R., 1964. Long period variations of the geomagnetic field, *Bul. seism. Soc. Am.,* **54,** 2243–2270.

Dormy, E., Valet, J.-P. & Courtillot, V., 2000. Numerical models of the geodynamo and observational constraints, *Geochem., Geophys., Geosys.,* **1,** doi:10.1029/2000GC000062.

Elsasser, W., Ney, E. & Winckler, J., 1956. Cosmic-ray intensity and geomagnetism, *Nature,* **178,** 1226–1227.

Finlay, C. & Jackson, A., 2003. Equatorially dominated magnetic field change at the surface of Earth's core, *Science,* **300,** 2084–2086.

Gubbins, D., 1975. Numerical solutions of the hydromagnetic dynamo problem, *Geophys. J. R. astr. Soc.,* **42,** 295–305.

Gubbins, D., 1987. Mechanism for geomagnetic polarity reversals, *Nature,* **326,** 167–169.

Gubbins, D., 1998. Interpreting the paleomagnetic field, in *The Core-Mantle Boundary Region,* Vol. 28, pp. 167–182, Geodynamics Series, American Geophysical Union.

Gubbins, D. & Gibbons, S., 2004. Low Pacific secular variation, in *Timescales of the Paleomagnetic Field,* Vol. 145, pp. 279–286, Geophysical Monograph, American Geophysical Union.

Gubbins, D., Jones, A. & Finlay, C., 2006. Fall in Earth's magnetic field is erratic, *Science,* **312,** 900–902.

Hollerbach, R., 2003. The range of timescales on which the geodynamo operates, in *Earth's Core: Dynamics, Structure, Rotation,* Vol. 31, pp. 181–192, Geodynamics Series, American Geophysical Union.

Hongre, L., Hulot, G. & Khokhlov, A., 1998. An analysis of the geomagnetic field over the past 2000 years, *Phys. Earth planet. Inter.,* **106,** 311–335.

Hulot, G. & Bouligand, C., 2005. Statistical palaeomagnetic field modelling and symmetry considerations, *Geophys. J. Int.,* **161,** 591–602.

Hulot, G. & Gallet, Y., 1996. On the interpretation of virtual geomagnetic pol (VGP) scatter curves, *Phys. Earth planet. Inter.,* **95,** 37–53.

Hulot, G. & LeMouël, 1994. A statistical approach to Earth's main magnetic field, *Phys. Earth planet. Inter.,* **82,** 167–183.

Hulot, G., Eymin, C., Langlais, B., Mandea, M. & Olsen, N., 2002. Small-scale structure of the geodynamo inferred from Oersted and Magsat satellite data, *Nature,* **416,** 620–623.

Jackson, A., Jonkers, A.R.T. & Walker, M.R., 2000. Four centuries of geomagnetic secular variation from historical records, *Phil. Trans. R. Soc. Lond.,* A, **358,** 957–990.

Johnson, C. & Constable, C., 1998. Persistently anomalous pacific geomagnetic fields, *J. geophys. Res.,* **25,** 1011–1014.

Kono, M. & Roberts, P., 2002. Recent geodynamo simulations and observations of the geomagnetic field, *Rev. Geophys.,* **40,** 1013, doi:10.1029/2000RG000102.

Kono, M. & Tanaka, H., 1995. Mapping the Gauss coefficients to the pole and the models of paleosecular variation, *J. Geomag. Geoelectr.,* **47,** 115–130.

Korte, M. & Constable, C., 2005a. The geomagnetic dipole moment over the last 7000 years - new results from a global model, *Earth planet. Sci. Lett.,* **236,** 348–358.

Korte, M. & Constable, C.G., 2005b. Continuous geomagnetic field models for the past 7 millennia: 2. CALS7K, *Geochem., Geophys., Geosys.,* **6,** Q02H16, doi:10.1029/2004GC000801.

Korte, M., Genevey, A., Constable, C.G., Frank, U. & Schnepp, E., 2005. Continuous geomagnetic field models for the past 7 millennia: 1. a new global data compilation., *Geochem., Geophys., Geosys.,* **6,** Q02H15, doi:10.1029/2004GC000800.

Laj, C., Mazaud, A., Weeks, M., Fuller, M. & Herrero-Bervera, E., 1991. Geomagnetic reversal paths, *Nature,* **351,** 447.

Lowes, F., 1974. Spatial power spectrum of the main geomagnetic field, and extrapolation to the core, *Geophys. J. R. astr. Soc.,* **36,** 717–730.

Masters, G., Johnson, S., Laske, G. & Bolton, H., 1996. A shear-wave velocity model of the mantle, *Phys. Trans. Roy. Soc. Lond.,* **354,** 1385–1411.

McElhinny, M., 2004. Geocentric axial dipole hypothesis: a least squares perspective, in *Time-scales of the Paleomagnetic Field,* Vol. 145, pp. 1–12, Geophysical Monograph, American Geophysical Union.

McElhinny, M.W. & Senanayake, W.E., 1982. Variations in the geomagnetic dipole: I. The past 50 000 years, *J. Geomag. Geoelectr.,* **34,** 39–51.

McFadden, P., Merrill, R. & McElhinny, M., 1988. Dipole/quadrupole family modeling of paleosecular variation, *J. geophys. Res.,* **93,** 11 583–11 588.

Olson, P., 2002. The disappearing dipole, *Nature,* **416,** 591–594.

Quidelleur, X. & Courtillot, V., 1996. On low degree spherical harmonic models of paleosecular variation, *Phys. Earth planet. Inter.,* **95,** 55–77.

Riedel, K. & Siderenko, A., 1995. Minimum bias multiple taper spectral estimation, *IEEE Trans. Signal Process.,* **43,** 188–195.

Solanki, S., Usoskin, I., Kromer, B., Schüssler, M. & Beer, J., 2004. Unusual activity of the sun during recent decades compared to the previous 11 000 years, *Nature,* **431,** 1084–1087.

Stuiver, M., Braziunas, T., Becker, B. & Kromer, B., 1991. Climatic, solar, oceanic, and geomagnetic influence on Late-Glacial and Holocene atmospheric $^{14}C/^{12}C$ change, *Quatern. Res.,* **35,** 1–24.

Tauxe, L., 2006. Long-term trends in paleointensity: the contribution of DSDP/ODP submarine basaltic glass collections. *Phys. Earth Planet. Inter.,* Vol. 156, Issues 3–4, pp. 223–241.

Tauxe, L. & Kent, D., 2004. A simplified statistical model for the geomagnetic field and the detection of shallow bias in paleomagnetic inclinations: was the ancient magnetic field dipolar?, in *Time-scales of the Paleomagnetic Field,* Vol. 145, pp. 101–115, Geophysical Monograph, American Geophysical Union.

Valet, J.-P., 2003. Time variations in geomagnetic intensity, *Rev. Geophys.,* **41,** doi:10.1029/2001/RG000104.

Yang, S., Odah, H. & Shaw, J., 2000. Variations in the geomagnetic dipole moment over the last 12000 years, *Geophys. J. Int.,* **140,** 158–162.

Young, R., 1974. Finite amplitude thermal convection in a spherical shell, *J. Fluid Mec.,* **63,** 695–721.